S-wave velocity uppermost mantle structure beneath the Central Mariana subduction zone inferred from ambient noise tomography

Tae-shin Kim[1], Sung-Joon Chang[1]

[1] Department of Geophysics, Kangwon National University, Chuncheon, South Korea, tskim@kangwon.ac.kr

Abstract

Understanding the structure of subduction zones is essential for elucidating water transport mechanisms into the mantle, as the subducting slab serves as the primary conduit for water entering the deep Earth. The Central Mariana subduction zone, where some of the oldest oceanic crust is subducting, exhibits key geophysical processes, including forearc serpentinization evidenced by serpentinite mud volcanoes, arc volcanism driven by slab-derived volatiles, and the formation of new oceanic lithosphere at back-arc spreading centers. In this study, we estimated fundamental-mode Rayleigh-wave group- and phase-velocity dispersion curves for periods ranging from 6 to 35 s, first-overtone Rayleigh-wave phase-velocity dispersion curves for 5–13 s, and fundamental-mode Love-wave group- and phase-velocity dispersion curves for periods of 7–18 s. These estimates were derived using continuous seismic data from 32 ocean-bottom seismometers and 19 island stations. Additionally, we applied the three-station interferometry to determine group and phase velocities between asynchronous station pairs. By jointly inverting the multimode Rayleigh-wave dispersion curves, we constructed an S-wave velocity model with resolutions down to 100 km depth. Furthermore, by jointly inverting Rayleigh- and Love-wave dispersion data, we computed a radial anisotropy model down to crustal depths. For Rayleigh-wave inversion, we employed a 3D reference model based on Crust1.0 and ak135, where topography and Moho depth were modified using the ETOPO1 model and seismic refraction data. For Love-wave inversion, we used a slightly modified version of the 3D reference model used in the Rayleigh-wave inversion, with adjusted velocity values. The resulting velocity model reveals prominent low-velocity anomalies along the subducting slab down to ~40 km depth, indicative of serpentinization, as well as beneath the volcanic arc (60–90 km depth) and the back-arc spreading center (10–30 km depth). Notably, we observe a structural connection between the low-velocity anomalies beneath the volcanic arc and the back-arc spreading center, suggesting a pathway for material and fluid transport. These findings provide new insights into the role of subduction dynamics in water cycling and mantle processes beneath the Central Mariana subduction zone.

Study area

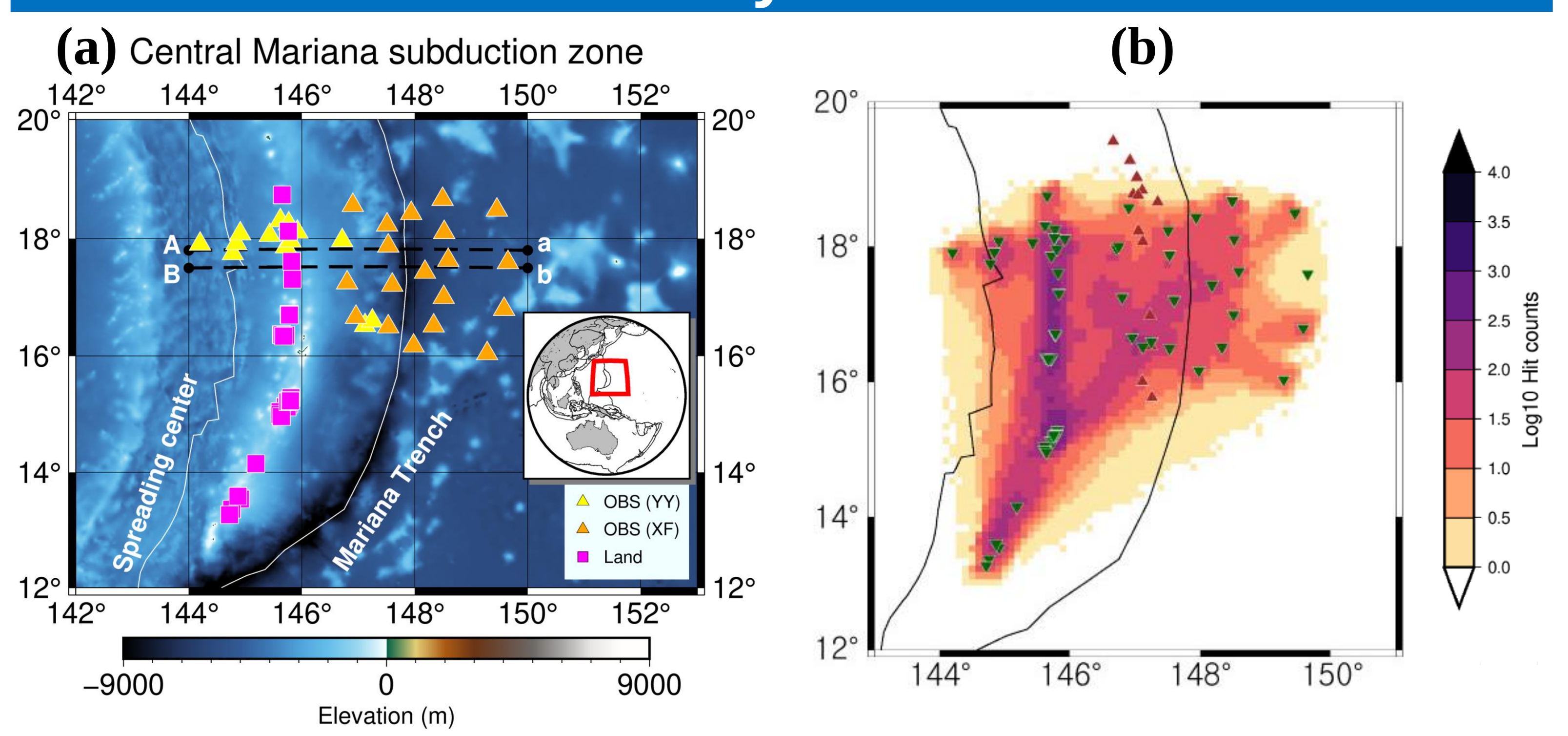

Figure 1. (a) Map of the stations used in this study and (b) hit counts for raypath obtained by noise cross-correlations.

Noise reduction

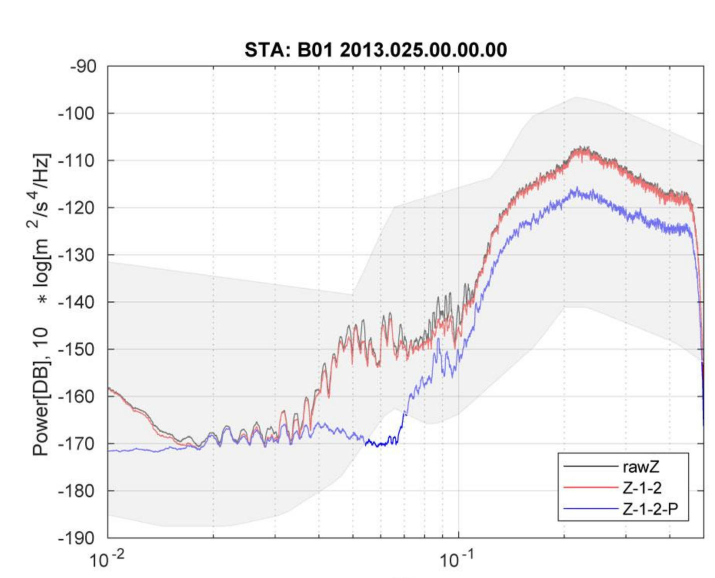

$$A_{XY} = \gamma_{XY}(f)\sqrt{\frac{G_{XX}(f)}{G_{YY}(f)}}$$

A_{XY}: transfer function between two channels

$\gamma_{XY}(f)$: coherence function

$G(f)$: auto spectral density

Figure 2. Example 24hr power spectral density for station B01. The raw vertical channel (Z), tilt-corrected (Z-1-2) and tilt & pressure-corrected vertical (Z-1-2-P) are shown.

- The transfer function between each component is calculated to remove tilt & compliance noise recorded by the ocean-bottom seismometer (Crawford & Webb, 2000).
- To measure the fundamental- and overtone-mode group velocities, we consider both tilt-corrected and tilt- & pressure-corrected data.

Conclusions

- Isotropic and radial anisotropic Vs model are constructed using Rayleigh- and Love-wave obtained from two- and three-station interferometry.
- Low-velocity anomalies are found beneath the Mariana trench, volcanic arc, and Back-arc, with the weak anomaly between the arc and backarc possibly reflecting a slab–backarc connection that diminished as the trench retreated.

Two-station interferometry

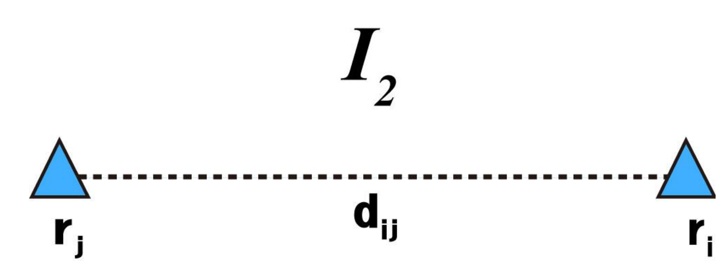

The empirical Green's function $\widehat{G}_2(r_i, r_j)$ between synchronous receiver pair is computed from the noise cross-correlation $C_2(r_i, r_j)$.

Fig. 3. Schematic illustration of the conventional ambient noise tomography I_2.

Three-station interferometry

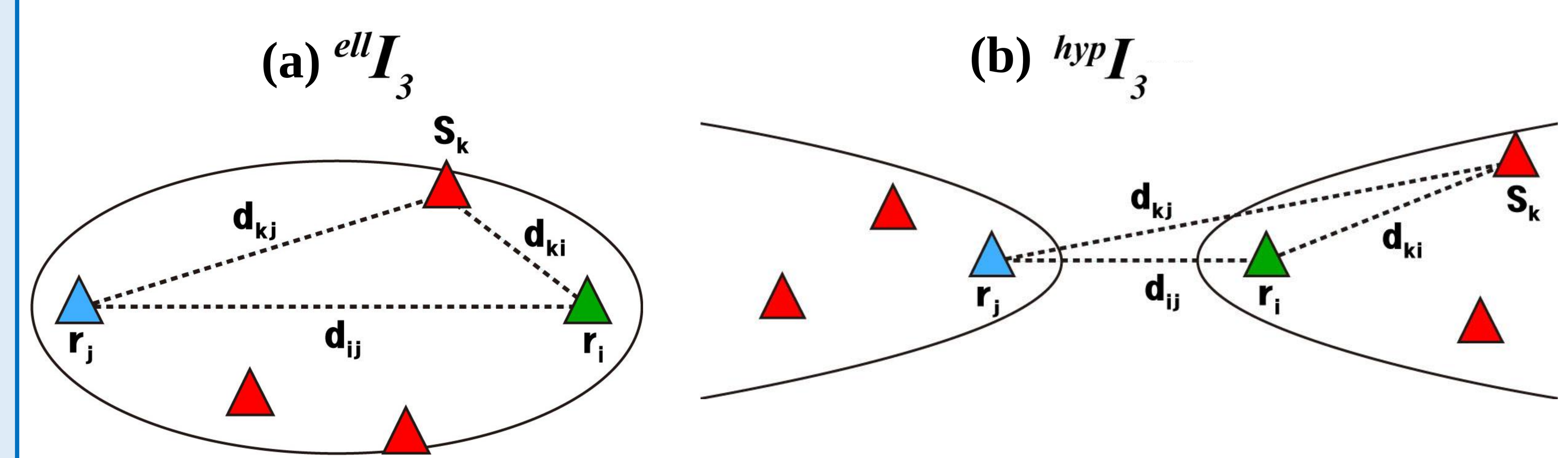

Fig. 4. Schematic illustration of the three-station interferometry I_3. (a) The case of ${}^{ell}I_3$, where the source station S_k is located within the elliptical stationary-phase zone. (b) The case of ${}^{hyp}I_3$, where S_k is located within the hyperbolic stationary-phase zone. The stations r_i and r_j serve as the foci of the ellipse and hyperbola, respectively.

- To compute the empirical Green's function $\widehat{G}_3(r_i, r_j)$ between asynchronous station pair, we apply a three-station interferometry method using two receiver stations and one source station. The source station is required to have recording periods that overlap with both receiver stations.
- The ${}^{ell}I_3$ satisfies Eq (1), and the corresponding ${}^{ell}C_3(r_j, r_i; S_k)$ is computed by convolving $C_2(S_k, r_j)$ and $C_2(S_k, r_i)$. The ${}^{hyp}I_3$ satisfies Eq (2), and the corresponding ${}^{hyp}C_3(r_j, r_i; S_k)$ is computed by cross-correlating $C_2(S_k, r_j)$ and $C_2(S_k, r_i)$. The parameter α represents the degree of bias.

$$d_{ki} + d_{kj} \le (1+\alpha)d_{ij} \quad (1)$$

$$|d_{ki} - d_{kj}| \ge (1-\alpha)d_{ij} \quad (2)$$

Resolution test

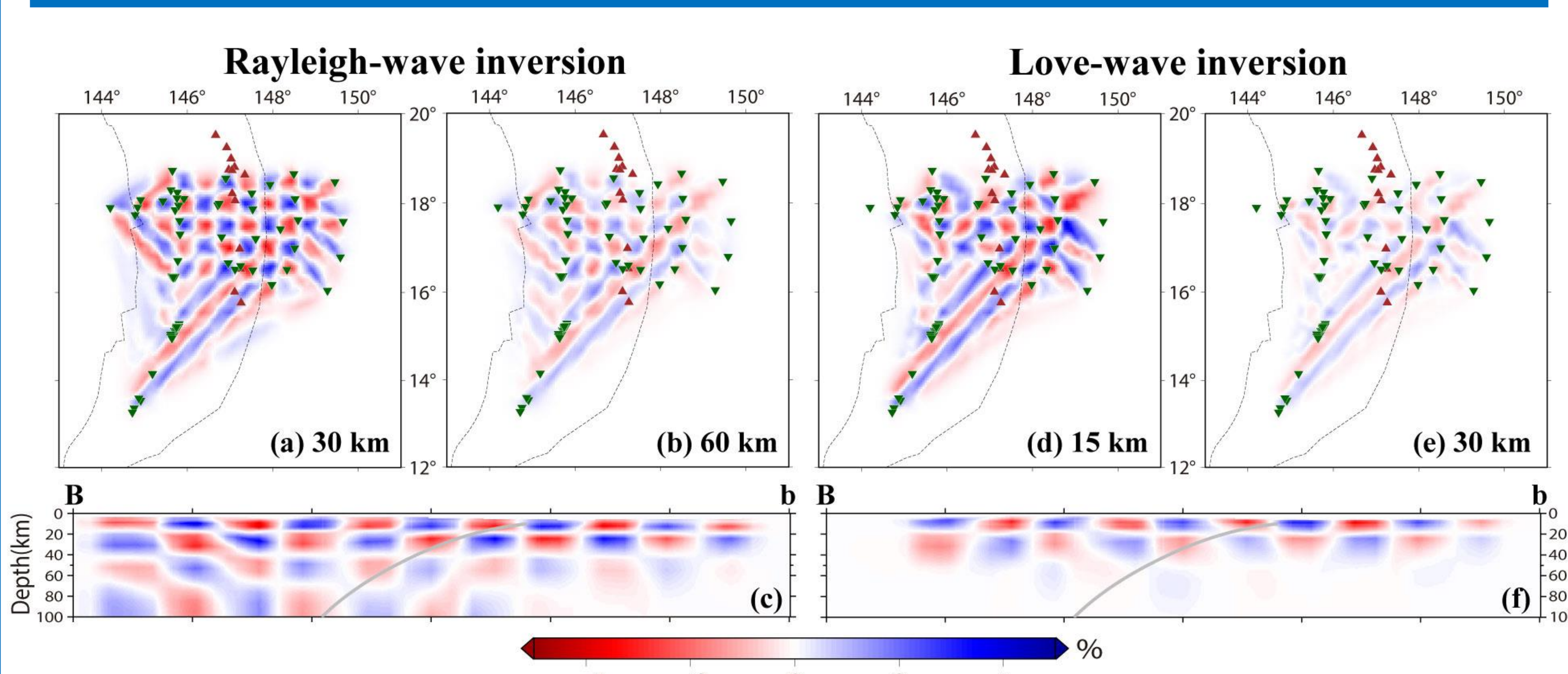

Fig. 5. Horizontal checkerboard test results for the Rayleigh-wave inversion model are shown at depths of (a) 30 km and (b) 60 km, and the vertical test result is shown in (c). For the Love-wave inversion model, horizontal test results are shown at (d) 15 km and (e) 30 km, with the vertical test result in (f).

References

Isotropic Vs model

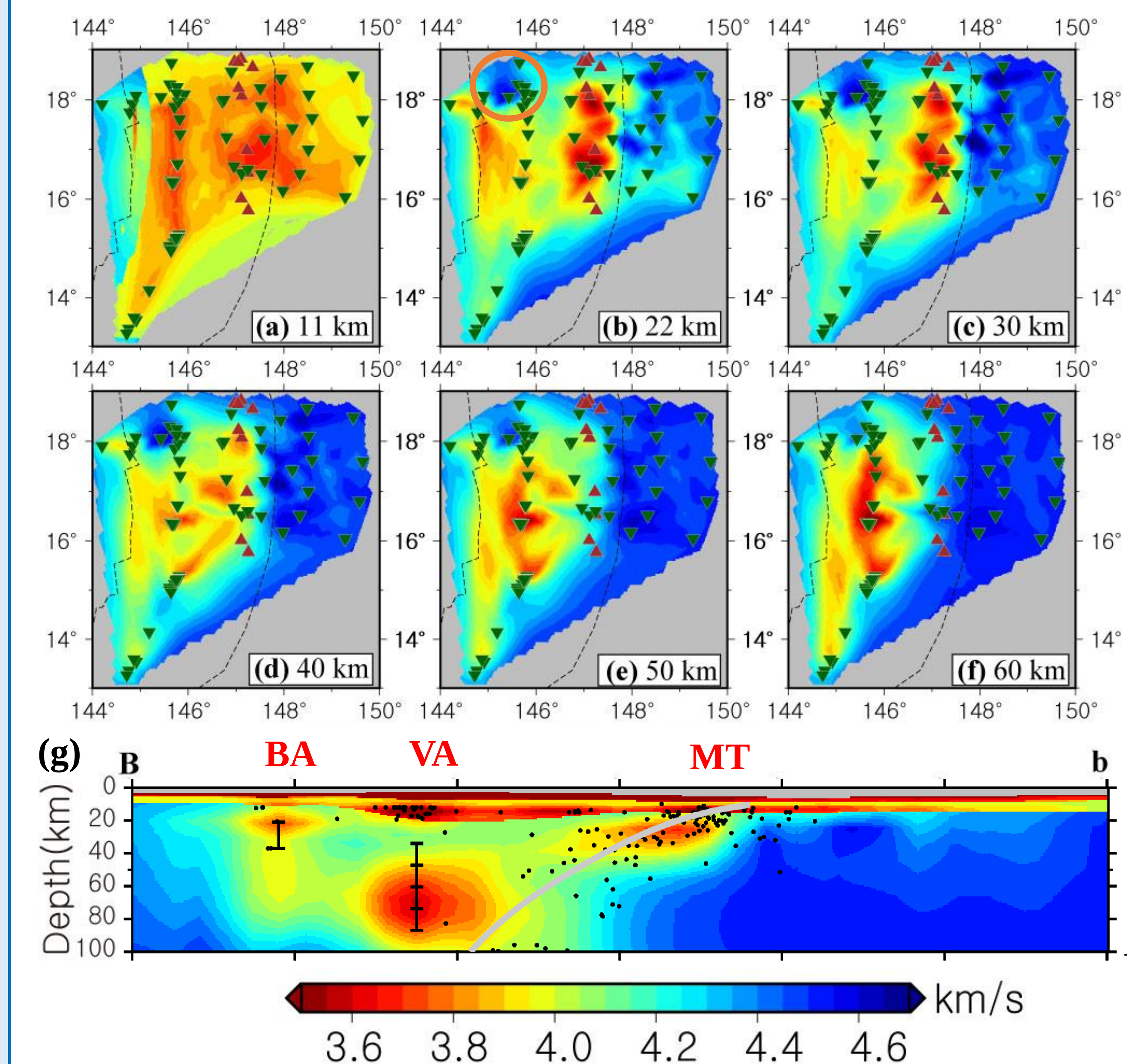

Fig. 6. The results of inversion using fundamental- and 1st overtone mode Rayleigh-wave dispersion curves. Each figure shows the horizontal slices of S-velocity model at (a) 11, (b) 22, (c) 30, (d) 40, (e) 50, (f) 60 and (g) the vertical slices along longitude 144°-150° and latitude 17.5°. Red triangles indicate mud volcanos.

- Low velocities are observed along the back-arc spreading center (BA) and volcanic arc (VA) as well as near the Mariana trench (MT).
- Isotropic Vs results are align with the magma equilibration depths (black lines in Fig.6g) estimated from thermobarometry (Kelley et al., 2010).
- The weak anomalies between BA and VA may reflect a past where the slab and back-arc were more closely connected (Wu et al., 2016), allowing fluid transport to the spreading center before trench retreat weakened this pathway.

Radial anisotropy model

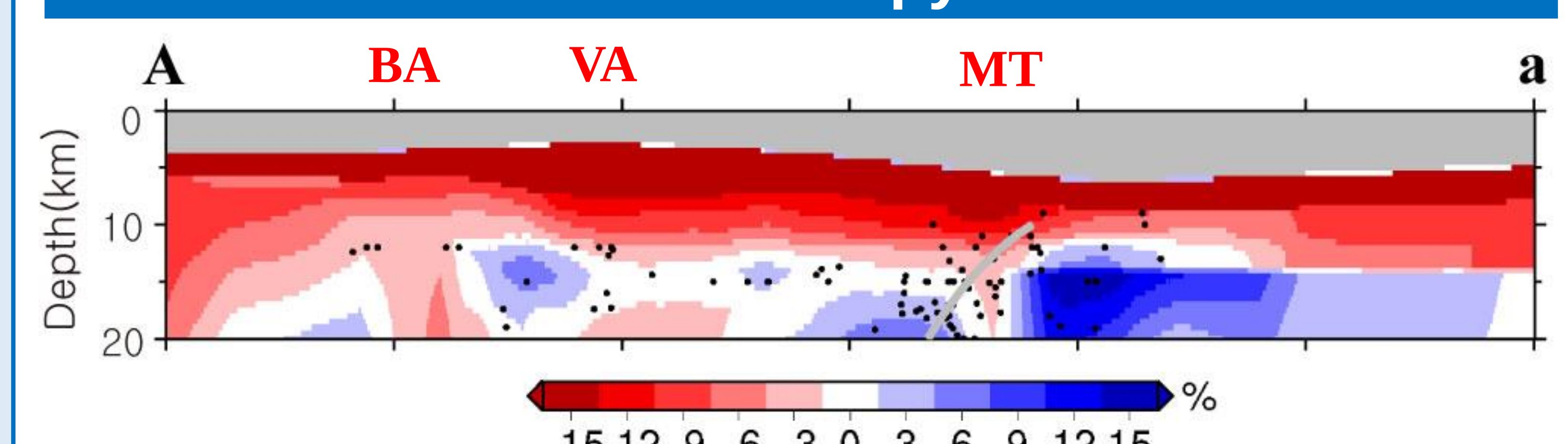

Fig. 7. The result of radially anisotropy perturbations from Rayleigh- and Love-wave inversion. The vertical slice extends along longitude 144°–150° and latitude 17.8°.

- Positive radial anisotropy is observed bewteen BA and VA just beneath the Moho, possibly caused by cold lithosphere associated with initial back-arc rifting (orange circle in Fig. 6b and Fig.7).
- Negative radial anisotropy are predominantly observed at crustal depths, which may result from vertical dykes responsible for many seamounts and volcanos in this region.